Journal of Catalysis **205,** 7–15 (2002)
doi:10.1006/jcat.2001.3317, available online at http://www.idealibrary.com on IDEAL®

Decomposition of Nickel Formate on Sol–Gel Alumina and Characterization of Product by X-Ray Photoelectron and TOF-SIMS Spectroscopies

A. Nemati Kharat,* P. Pendleton,† A. Badalyan,† M. Abedini,* and M. Mohammadpour Amini*,[1]

*Department of Chemistry, University of Tehran, P.O. Box 14155-6455, Tehran, Iran; and †Porous Materials Research Group, School of Chemical Technology, University of South Australia, Mawson Lakes, South Australia 5095, Australia

Received September 5, 2000; revised May 16, 2001; accepted June 13, 2001

Samples of nickel-supported alumina were prepared from sol–gel and non-sol–gel alumina by impregnation of aqueous solution of nickel formate and the decomposition behavior of the nickel formate on alumina was then followed by combined thermal analysis and infrared spectroscopy. The decomposition products were characterized by X-ray photoelectron spectroscopy, time-of-flight secondary-ion mass- spectroscopy, and scanning electron microscopy. The surface areas and pore distributions were measured by BET. Nickel formate was found to decompose over a wide temperature range owing to its interaction with the alumina. The surface area of the sol–gel alumina after nickel loading increased whereas the non-sol–gel alumina remained unchanged. The products were amorphous, and they had a pore distribution in the mesoporous region. The nickel species existed as nickel aluminate, unsupported nickel oxide, stoichiometric nickel oxide, and metallic nickel. The nickel species were uniformly distributed on the surface. The particles agglomerated at the submicron level; no nickel species was found on the surface.

Key Words: **sol–gel alumina; nickel formate; thermal analysis; XPS; TOF-SIMS.**

1. INTRODUCTION

Supported nickel systems have been extensively been investigated since the pioneering work of Hill and Selwood (1), with much of the interest in supported nickel catalysts arising from the widespread applications of these systems in hydrogenation (2, 3), steam-reforming reactions (4–6), reductive amination of alcohols (7), hydrodechlorination (8–10), partial oxidation (11, 12), and methanation (13–16). Among such applications, the last application is particularly attractive in exhaust-gas regeneration technology (17) in the light of increasing environmental concern over the use of fossil fuels.

Depending on the application, supported nickel catalysts are usually prepared from nickel salts and an oxide by impregnation or co-precipitation methods (18). Apparently, the nature and concentration of the catalyst metal precursor (19, 20), the pH of the aqueous slurry support, the isoelectric point of the support, and the pH at which surface polarization occurs are the most important variables in the preparation of supported nickel catalysts (21). In addition, the nature of compounds formed between the nickel and the support (22–26), total pore volume, and metal surface area varies with the preparative conditions (27, 28). Interestingly, other studies have shown that the nickel support interaction has significant impact on final catalytic activity (29–32). For instance, in the steam-reforming reaction, the participation of monodispersed nickel atoms (which are generated from the reduction of surface nickel aluminate in a fully reduced catalyst) has been attributed to the selectivity of carbon monoxide (33). Several investigations have addressed the interaction of nickel and alumina (34–38); these studies have concluded that both the magnitude and type of interaction depended on several distinctly different physical properties. Although the effect of nickel loading, calcination temperature, and alumina structure have been investigated in nickel–alumina catalysts, the interaction of the support surface itself with nickel remains less well understood. The Brunell adsorption model, which is used to explain metal and support interactions, only considers electrostatic interactions and does not take into account the heterogeneity of the surface hydroxyl groups (21). The heterogeneity of the surface can have a great impact on the specific adsorption of the catalyst. An understanding of the chemistry of the metal-support interface in relation to catalytic performance (39) is of importance to the design of a catalyst for a specific reaction. Furthermore, nickel nitrate, which is widely used for the preparation of supported nickel catalysts, decomposes to nickel oxide in the calcination process (40–42). In contrast, nickel formate readily decomposes to metallic nickel (43). In using nickel formate as a precursor, metallic nickel can be introduced on a support at a relatively low temperature; the synthesis of nickel-supported catalysts is an essentially mild route.

[1] To whom correspondence should be addressed. Fax: 0098-21-6405141.

0021-9517/02 $35.00

This fact is useful for providing a further understanding of nickel support interaction as well as of the rapid thermal deactivation of conventional catalysts.

Sol–Gel-derived oxides are known to be endowed with a hydroxyl-rich surface; they exhibit different behaviors compared with oxides prepared by conventional techniques (44, 45). Porous aluminas with varieties of physical properties have been prepared by the sol–gel method and these are widely used as catalyst supports (46). As a contribution to this rapidly growing field of catalysis, this paper details the decomposition of nickel formate on the sol–gel-derived alumina.

2. EXPERIMENTAL

2.1. Sol–Gel Preparation of Alumina

Aluminum-2-butoxide was synthesized from aluminum and 2-butanol according to the general method for preparing aluminum alkoxides. A mixture of 22 ml water and 300 ml 2-butanol was added dropwise to 1600 ml of a 0.25 M solution of the aluminum-2-butoxide in 2-butanol at 75°C. The resulted milky emulsion was stirred at 75°C for 3 h. The mixture was kept at this temperature for 100 h. The white solid that separated was aged for another 48 h. The solid was collected and dried at 110°C for 24 h. It was pulverized and then calcined in air for 15 h at 800°C. This alumina was used for the preparation of sample A.

2.2. Preparation of Catalysts

Commercial aluminas were obtained from the Aldrich Chemical Company and were calcined at 800°C for 15 h. Sample B was prepared from sol–gel-derived alumina (*in situ*) and catalysts C, D, and E were prepared from commercial aluminas with acidic, neutral, and basic surface. Samples A, C, D, and E were prepared by impregnation of aluminas with an aqueous solution of nickel formate. The mixtures were dried at 80°C on a water bath. The resulting green powders were calcined in air at 230°C for 24, 48, and 72 h (Table 1). The completion of the decomposition of nickel formate was monitored by the absence of the nickel formate characteristic peaks in the infrared spectrum.

For the preparation of sample B, an aqueous solution of nickel formate was added to the alumina sol, which had been prepared from the hydrolysis of aluminum-2-butoxide. The gel similarly was treated and it was calcined at 800°C for 15 h. The nickel content of the catalysts was kept at 7 wt%. The physical properties and experimental details are presented in Table 1.

2.3. Characterization

In the gas adsorption measurements, ultra-high-purity nitrogen gas (99.999%) was adsorbed volumetrically on either the support or the catalyst/support at −196°C in a stainless-steel automatic volumetric adsorption apparatus (47). The level of liquid nitrogen surrounding the sample was ±0.3 mm. The samples were degassed in a turbo-molecular and rotary pumping system in tandem, which had a background pressure <0.7 mPa. The sample weights were corrected for weight loss from degassing or drying. The pore distributions for diameters in the 10–500 Å range were calculated by the Barrett–Joyner–Halenda (BJH) method. Thermal analysis was performed on a Rheometric Scientific STA-1500 instrument with heating rate of 10°C/min in air or nitrogen; the samples were dried at 80°C. X-ray diffraction (XRD) patterns were recorded on a Phillips PW-1800 diffractometer equipped with Cu Kα radiation; 2θ scans were performed from 5° to 90° at a 3°/min speed. Infrared spectra were recorded as KBr disks on a Bio-Rad FTS- 65 computer-operated spectrometer (wave number resolution = 4 cm^{-1}). The samples and KBr were predried in a vacuum oven at 100°C before the spectra were recorded. The X-ray photoelectron spectra (XPS) were obtained on a PHI 5600 XPS spectrometer (effective resolution = 0.8 eV). The spectrometer was equipped with a hemispherical energy analyzer and a magnesium anode as the X-ray radiation source (Mg Kα = 1253.6 eV). The powder samples were isostatically cold-pressed by a small stainless-steel cylinder, mounted on a sample holder, placed in the prevacuum chamber, and then transferred to the main vacuum chamber. The residual pressure in the main vacuum chamber during data collection was kept below 7×10^{-9} Torr. For

TABLE 1

Details of the Samples Used in This Investigation

Catalyst	Alumina type	Ni loading method	S. A. before Ni loading (m^2/g)	S. A. after Ni loading (m^2/g)	Decomp. time (h)	Color
A	sol–gel	Impreg.	203	250	72	Pale green
B	sol–gel	In situ SG	—	125	—	Blue
C	acidic	Impreg.	155	136	48	Gray
D	neutral	Impreg.	155	136	24	Black
E	Basic	Impreg.	155	130	24	Black

each of the spectral regions of interest, a number of scans were signal-averaged so as to give a sufficiently low signal-to-noise ratio. Binding energies were corrected by charge referencing to the carbon 1s line at 284.9 eV. A Gaussian–Lorentzian curve-fitting program (Gaussian : Lorentzian = 4 : 1) was used to deconvolute overlapping peaks. TOF-SIMS spectra were obtained in the static mode on a PHI TRIFT II TOF-SMIS system (ion dose = 10^{15} ion/cm^2) using a 15-kV and 25-kV pulsed Ga source for the high-mass-resolution spectra and high-special-resolution images. Electron microscopy was performed on a Phillips XL-30 SEM.

3. RESULTS AND DISCUSSION

BET surface areas of the samples before and after impregnation are given in Table 1. The noticeable decrease in areas of samples C, D, and E after nickel loading is due to the alumina weight percent reduction in the samples; this has also been observed in the preparation of γ-alumina-supported nickel catalysts (25). Sample B, which has the least surface area among the five samples, clearly demonstrates influence of the method of preparation on the physical properties. In sample B, which was prepared by the addition of nickel formate to alumina sol, the nickel-containing species were partially buried in the alumina surface; at a calcination temperature of 800°C, the sample texture also changed. The sample prepared from the sol–gel-derived alumina, A, shows a completely different behavior than those of samples C, D, and E. After nickel loading, the surface area was increased from 203 to 250 m^2/g. As the surface of the sol–gel-derived alumina is rich in hydroxyl groups, the decomposition of nickel formate in the pores, dehydroxylation, and evolution of gases during decomposition of nickel formate are probably related to the increment in surface area. The pore size distributions of all the samples, calculated from the N_2-adsorption isotherm at 77 K by using the method of Barrett, Jayer, and Halenda (48), shows a flat baseline up to the 100-nm pore region. This behavior has been interpreted by others in terms of an efficient blocking of the pore support by the nickel species (25). The nitrogen adsorption–desorption isotherms for sample A are shown in Fig. 1. This material displays a type IV isotherm according to the classification of Brunauer, Deming, Deming, and Teller (49); the bulk of pore volume arises from mesopores. Further evidence for the different behavior of sample A comes from the total time required for the complete decomposition of nickel formate. The characteristic peaks of nickel formate in the infrared spectrum of sample A are still noticeable after 60 h of heating at 230°C. This time is markedly higher than that for catalysts D and E but is similar to that of catalyst C. Possibly, in the acidic alumina-support catalysts A and C, some degree of interaction between nickel formate and supports exists which stabilizes the nickel formate to some extent.

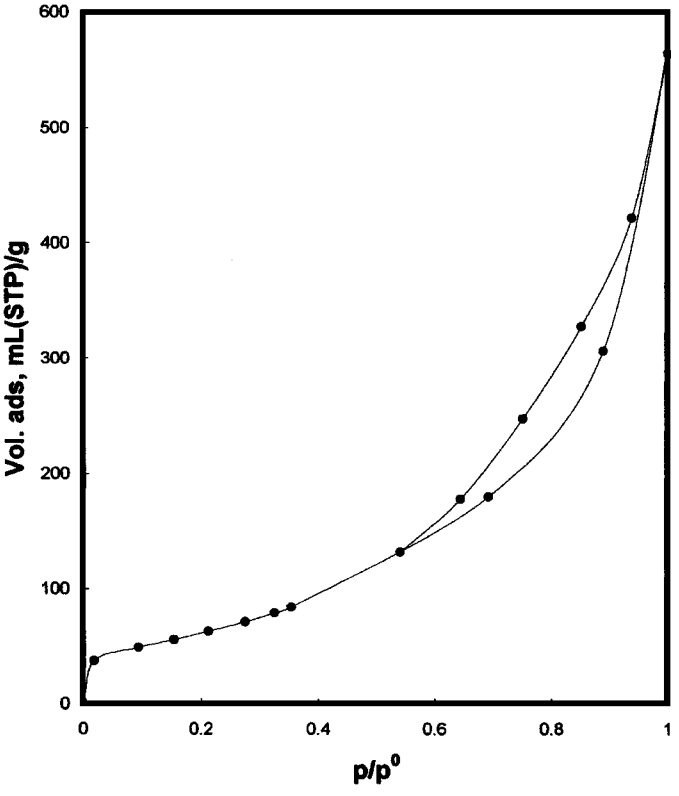

FIG. 1. Nitrogen adsorption–desorption isotherms of sample A at 77 K.

Thermogravimetric analysis (TGA) and differential scanning calorimetry (DSC) were employed to investigate decomposition behavior of nickel formate on alumina during the course of heat treatment in air and nitrogen atmospheres. The DSC and TGA curves of pure nickel formate, sample A and sample E, are depicted in Fig. 2. The TGA curve of the nickel formate impregnated on basic alumina (Fig. 2b) shows about 6% weight loss upon heating to ~200°C. This weight loss is accompanied by an endothermic peak in the DSC curve that indicates that the weight loss is due to the dehydration of nickel formate. The distinct exothermic peak at ~285°C in the DSC curve with 9% weight loss in the TGA curve of sample E is associated with the decomposition of nickel formate. The thermal analysis of pure nickel formate (Fig. 2c) shows a similar behavior, but there are an extra exothermic peak at ~400°C in DSC curve and an increase in weight. This peak corresponds to the oxidation of nickel that results from decomposition of nickel formate. The thermogram of nickel formate impregnated on sol–gel alumina, A, on the other hand, is quite different; the DSC curve (Fig. 2a) shows a broad endothermic peak at ~100°C, which suggests that most of the weight loss is due primarily to the elimination of physically adsorbed water rather than chemically bound water. The DSC curve of sample A also shows a broad exothermic peak around 480°C, accompanied by a slight weight loss in the TGA curve. The nature of this exothermic peak is not clear at this

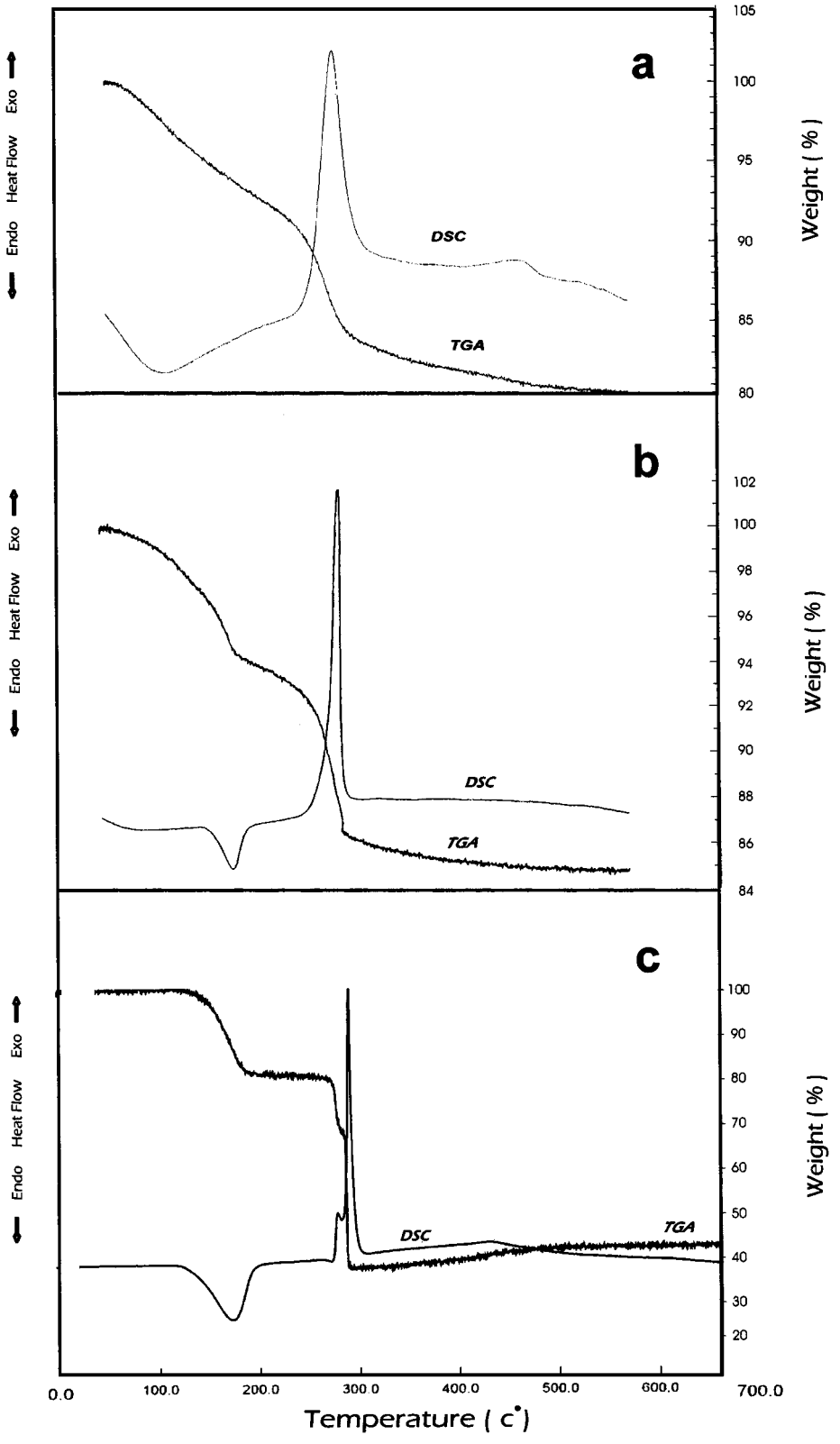

FIG. 2. DSC and TGA curves of (a) sample A, (b) sample E, and (c) pure nickel formate.

time. However, the simultaneous thermal analysis of the NiO/SiO_2 catalyst in hydrogen also reveals a broad exothermic peak at the same temperature; this feature is ascribed to the reduction of nickel oxide (50). In this context, the reduction of a portion of nickel oxide to nickel by trapped hydrogen in alumina, which is a known product of nickel formate decomposition, is tentatively suggested. Such high-temperature behavior should be very interesting and probably will change the whole picture of nickel formate decomposition on alumina. Analysis by a temperature program reduction apparatus coupled with a mass spectrometer (TPR-MS) could be helpful for clarifying this. Furthermore, when the simultaneous thermal analysis (STA) of sample A was carried out under nitrogen, identical curves were obtained with the same amount of weight loss, which corroborated the decomposition of nickel formate at 285°C. It is also obvious that the main exothermic peak in the DSC curve of sample A is broad as compared with similar DSC peaks for sample E or pure nickel formate. Apparently, there is a relationship between broadness of the DSC peaks and the times required for the complete decomposition of nickel formate on different aluminas. It seems that nickel formate on the sol–gel alumina decomposes in a broad temperature range due to the stronger interaction. Interestingly, the reaction and partial decomposition of nickel acetylacetonate by the catalytic action of the acidic sites of alumina surface has been reported (51).

The X-ray diffraction pattern of all samples was recorded; however, further insight into the interface could not be definitively obtained (22). The lack of crystallinity is probably due to the low nickel loading; such weak diffraction lines of Ni and NiO are not unusual in Ni/γ-alumina systems (17, 25, 40). The low crystallinity of the nickel/γ-alumina system has been attributed to the NiO/γ-alumina interaction (25).

As mentioned in Table 1, the nickel content of all samples is 7 wt%. This level leads to the formation of a monolayer of nickel on the surface of support. Obviously, it is possible to have several types of nickel species on the surface if the surface area is not large enough to be covered by monolayer. In order to establish the nature of the nickel species the in Ni/alumina system, X-ray photoelectron spectroscopy was applied to all samples. The binding energies of O 1s, Al 2p, and Ni $2p_{3/2}$ are listed in Table 2 before deconvolution.

TABLE 2

Binding Energies of O 1s, Al 2p, and Ni 2p for the Prepared Samples

Catalyst	O 1s	Al 2p	Ni $2p_{3/2}$ (main)	Ni $2p_{3/2}$ (satellite)
A	531.6	74.5	856.7	863.0
B	531.3	74.4	856.2	862.7
C	531.0	74.0	856.0	861.8
D	531.2	74.2	855.6	861.4
E	531.0	74.0	855.8	861.7

TABLE 3

Binding Energies and Contribution of Ni $2p_{3/2}$ after Deconvolution

Catalyst	Binding energies (contribution)			
A	^{M}853.2 (4%), [1.7]	^{G}855.7 (56%), [2.7]	^{U}856.8 (15%), [1.7]	^{N}857.8 (24%) [2.3]
B	^{U}854.8 (13%), [1.3]	^{G}855.8 (13%), [1.1]	^{N}856.6 (74%) [2.1]	
C	^{M}853.2 (10%), [1.8]	^{U}854.7 (33%), [1.9]	^{G}855.7 (23%), [1.5]	^{U}856.6 (34%) [1.9]
D	^{M}853.1 (9%), [1.1]	^{U}854.5 (14%), [1.6]	^{G}855.7 (77%) [2.2]	
E	^{M}853.4 (14%), [2.1]	^{U}855.0 (38%), [2.3]	^{U}856.8 (48%) [2.5]	

Note. M = metallic nickel, G = green stoichiometric nickel oxide, N = nickel aluminate, and U = unsupported nickel oxide. FWHM values are in brackets.

It is clear that the binding energies of O and Al in various samples are almost identical and they are close to those of Al_2O_3(52), but the binding energy of Ni $2p_{3/2}$ for sample A is higher in comparison with the non-sol–gel-derived alumina support. This clearly demonstrates the stronger interaction of Ni species and alumina, which leads to a shift of the main Ni $2p_{3/2}$ peak and its satellite to higher energies. This shift is lower for sample B. Probably the hydroxyl-rich surface of the sol–gel-derived alumina is responsible for the strong interaction. In fact, the formation of surface nickel aluminate at a temperature as low as 350°C from untreated γ-alumina was claimed to be the consequence of its hydroxyl groups (53). The binding energy data for all samples with the contribution percentage of each nickel-containing species in relation to the Ni $2p_{3/2}$ peaks after deconvolution are given in Table 3. For sample A, the Ni $2p_{3/2}$ and $2p_{1/2}$ core-level peaks are shown in Fig. 3 and its $2p_{3/2}$ deconvoluted peak in Fig. 4. It is interesting to highlight the high content of the nickel aluminate phase with binding energy of 856.6 eV with its satellite at 862.7 eV (24, 25, 54) on the surface of sample B, which was prepared by the addition of nickel formate to alumina in the sol stage. The peak with binding energy of 855.8 eV in this sample corresponds to the green stoichiometric nickel oxide and the peak at 854.8 eV is probably due to the unsupported nickel oxide (25). It is clear that the contribution of spinel phase is several times higher than that of other samples and there is no metallic nickel on the surface. This is not unexpected from the severity of the calcination process. In contrast, samples A, C, D, and E show a peak at about 853 eV, which is associated with the metallic nickel. A relatively constant binding energy of metallic nickel is indicative of a weak Ni-support interaction in comparison with that of the NiO-support interaction. Samples C and D additionally show green stiochiometric nickel oxide and unsupported nickel oxide. In sample E, the nickel-containing species on the surface are mainly in the form of unsupported

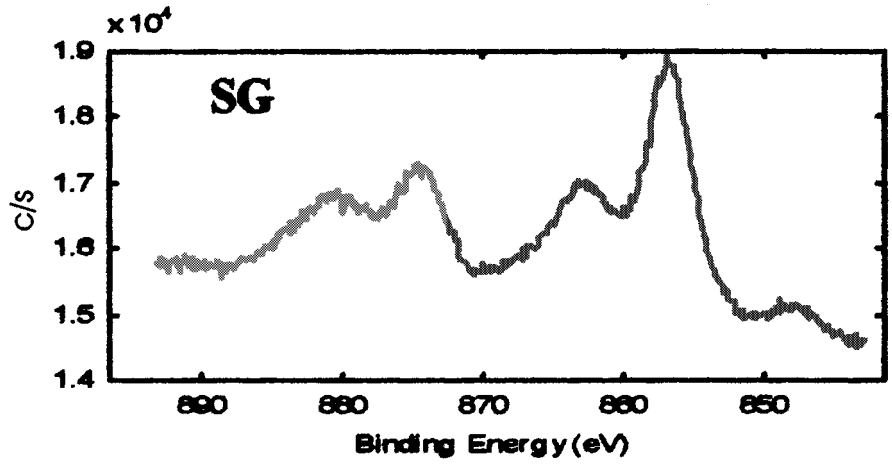

FIG. 3. XPS spectra of sample A for the Ni $2p_{3/2}$ and $2p_{1/2}$ levels.

nickel oxide with some metallic nickel. Analysis of sample A shows more interesting results. The peak at 857.8 eV with its satellite at 863.0 eV undoubtedly shows the presence of nickel aluminate on the surface (54). A little shift in Ni $2p_{3/2}$ binding energy can be attributed to the strong interaction of Ni and support and to a decrease in covalency and efficient dispersion of nickel species on support (22). The second major contributor to the Ni $2p_{3/2}$ peak of sample A is green stoichiometric nickel oxide, which appears at 855.7 eV; there is some unsupported nickel oxide and an insignificant amount of metallic nickel on the surface. The presence of the nickel aluminate phase is, to some extent, surprising, and to our knowledge, this is the lowest temperature (230°C) that has ever been observed for the formation of nickel aluminate. The strong interaction of the sol–gel-derived alumina with the nickel-containing species, which is obvious from the higher Ni $2p_{3/2}$ binding energy, is probably responsible for this low temperature of formation of nickel aluminate. Such processed nickel aluminate can readily be reduced to isolated nickel species, which could lead to an increase in activity and stability in the reforming reaction (17).

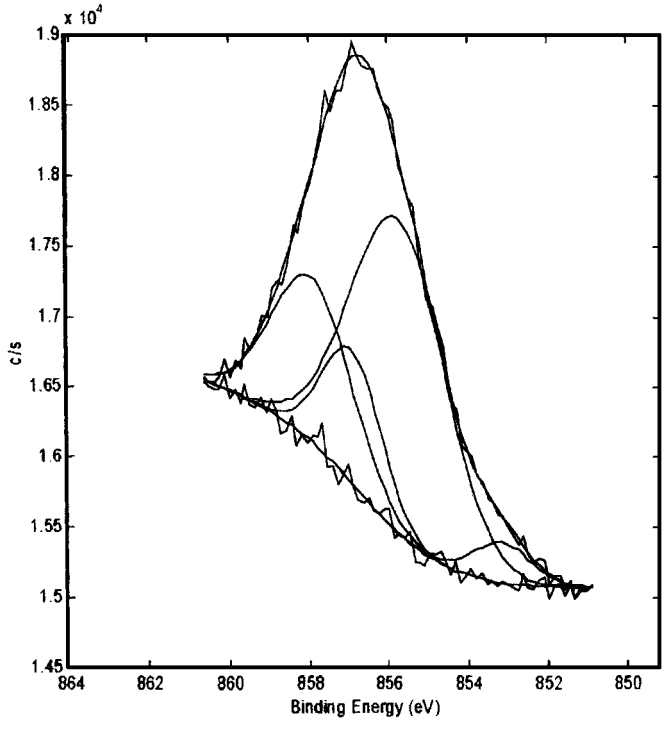

FIG. 4. XPS spectra of sample A for the Ni $2p_{3/2}$ level after deconvolution.

The atomic ratios of different elements on the surface of the prepared samples were calculated from the XPS spectra by accounting for atomic sensitivity factors and the inelastic mean free path of the electrons (55) (Table 4). Except for sample B, which, in some respect is not comparable with the other samples in the present study, sample A has the lowest Ni/Al ratio. It may be concluded that the mole fraction trends are consistent with nickel trapped in pores.

Besides the availability of nickel species on the surface, the homogeneity and uniform distribution of the active species are very important in catalytic performance. The distribution of the nickel species on alumina surface in the present study was investigated by TOF-SIMS. Figure 5 shows the TOF-SIMS image of nickel ion on the surface of samples A, C, D, and E. The Ni/Al ratio from different

TABLE 4

Surface Atomic Ratios of Oxygen, Aluminum, and Nickel for the Prepared Samples

Catalyst	O/Al	Ni/Al
A	2.23	0.148
B	1.96	0.066
C	2.06	0.216
D	2.38	0.350
E	2.14	0.190

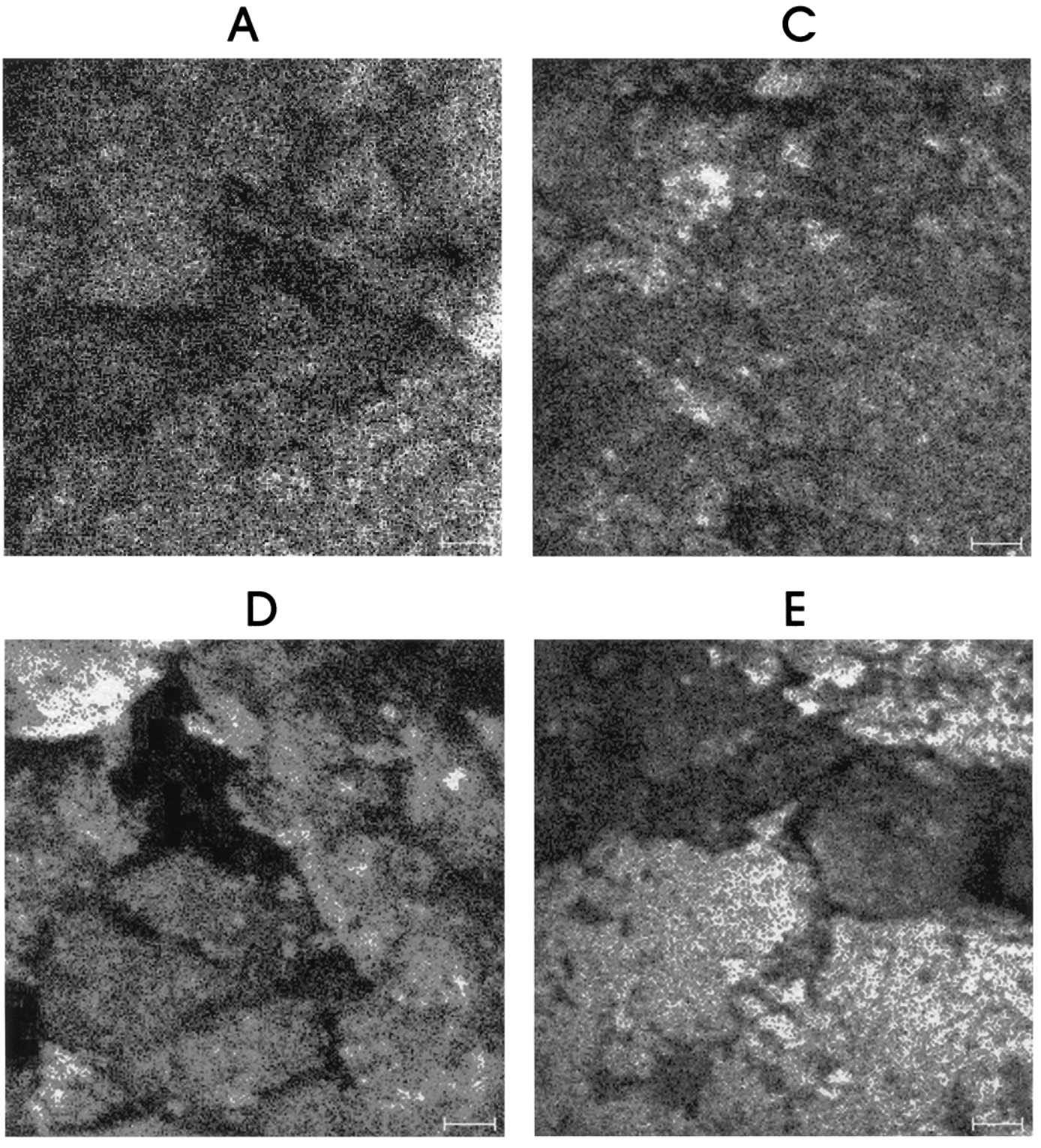

FIG. 5. TOF-SIMS images of samples A, C, D, and E. Gray indicates nickel.

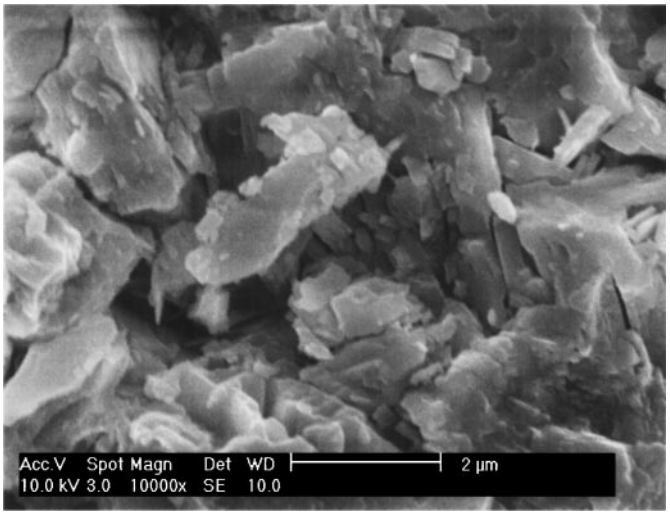

FIG. 6. SEM micrograph of sample E.

spots for the samples showed that the sample A, which has a constant Ni/Al ratio, has the best homogeneity and a fairly smooth distribution of nickel species, whereas the other samples exhibited very poor distribution of nickel species on the surface. Sample C, the acidic alumina support, also shows a better distribution of nickel species on the surface compared with D and E.

The morphology of samples was investigated by scanning electron microscopy. The micrograph of sample E (Fig. 6) shows large irregular particles. In contrast, sample A (Fig. 7) shows submicron agglomerated particles, which is typical of sol–gel-derived materials (56). No nickel particles were observed on the surface of either sample. Such a behavior for other sol–gel-derived alumina-supported metals have been reported. In another study, the TEM shows no Pt particles on the Pt/γ-Al_2O_3 catalyst prepared by the sol–gel

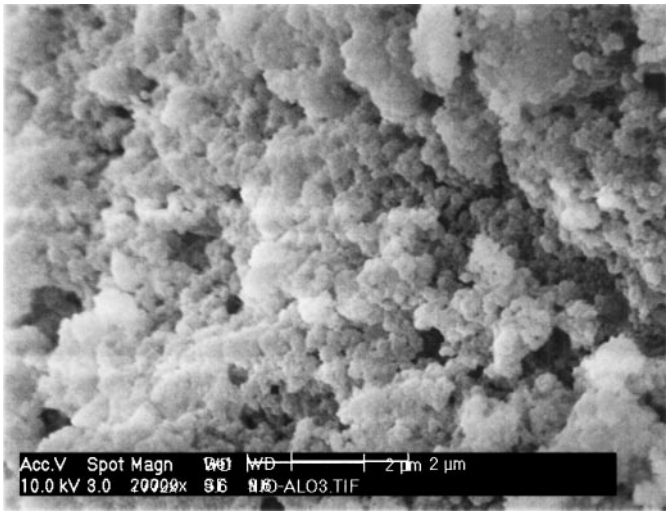

FIG. 7. SEM micrograph of sample A.

method (57). Apparently, in the sol–gel method, metal particles are buried or surrounded by alumina, and they are bound to the alumina so that they do not migrate to the surface. However, the nickel loading factor must be considered. The micrograph of highly loaded nickel sample, which was prepared from non-sol–gel alumina, shows large octahedra NiO whereas in the low nickel loading sample, NiO octahedra were encapsulated within the porous shell (25). In fact, recent studies show that the shell is a nonstoichiometric phase of nickel aluminate (58, 59). In the present study, the absence of NiO on the surface also can be attributed to the encapsulation of nickel in the porous sol–gel alumina and the formation of nickel aluminate shell on the surface. This interpretation is consistent with the results of XPS, which show a large amount of nickel aluminate in samples A and B. This is not surprising as the interaction of the metal and support is stronger due to low metal loading in addition to the tendency of the sol–gel-derived alumina to bind strongly with the metal.

4. CONCLUSION

The low-temperature decomposition of nickel formate on the sol–gel and non-sol–gel aluminas was investigated. The properties of materials obtained from the decomposition of nickel formate were compared with the same materials obtained from non-sol–gel alumina. Thermal analysis indicates that the decomposition behavior of nickel formate on sol–gel alumina is different. The sol–gel alumina exhibits a stronger interaction with nickel species. The strong interaction was attributed to the hydroxyl-rich surface of the sol–gel-derived alumina. The distribution of the nickel species on the sol–gel-derived alumina is very uniform, but the nickel species are buried in the alumina surface, which may not be available for catalytic purpose. Nickel aluminate readily forms on the sol–gel-derived alumina and covers the top layers of alumina. Thermal analysis of the sample prepared from the sol–gel-derived alumina shows interesting results at higher temperatures. Further work is in progress for the characterization of nickel species, which are formed at higher calcination temperatures.

ACKNOWLEDGMENTS

We are grateful to Dr. Angus Netting of the Ian Wark Research Institute, University of South Australia, for his help in recording the XPS and TOF-SIMS spectra. The generous financial support of the Research Council of Tehran University (Grant 514/1/392) is acknowledged. One of us (A.N.) thanks the Ministry of Higher Education of Iran for a travel grant to carry out part of his research in Australia.

REFERENCES

1. Hill, F. N., and Selwood, P. W., *J. Am. Chem. Soc.* **71**, 2522 (1949).
2. Tiainen, L. P., Arvela, P. M., and Salmi, T., *Catal. Today* **48**, 57 (1999).

3. Jacobs, J. P., Lindfors, L. P., Reintjes, J. G. H., Jylha, O., and Brongersma, H. H., *Catal. Lett.* **25**, 315 (1994).
4. Borowieek, T., Golebiowski, A., and Stasinska, B., *Appl. Catal. A* **153**, 141 (1997).
5. Yamazaki, O., Tomishige, K., and Fujimoto, K., *Appl. Catal. A* **136**, 49 (1996).
6. Sidjabat, O., and Trimm, D. L., *Top. Catal*. **11**, 279 (2000).
7. Dume, C., Holderich, W. F., *Appl. Catal. A* **183**, 167(1999).
8. Shin, E. J., and Keane, M. A., *Appl. Catal. B* **18**, 241 (1998).
9. Suzdorf, A. R., Morozov, S. V., Anshits, N. N., Tsiganova, S. I., and Anshits, A. G., *Catal. Lett*. **29**, 49 (1994).
10. Cesteros, Y., Salagre, P., Medina, F., and Sueiras, J. E., *Appl. Catal. B* **22**, 135 (1999).
11. Chu, Y. L., Li, S. B., Lin, J. Z., Gu, J. Z., and Yang, Y. L., *Appl. Catal. A* **134**, 67 (1996).
12. Miao, Q., Xiong, G. X., Sheng, S. S., Cui, W., Xu, L., and. Guo, X. X., *Appl. Catal. A* **154**, 17 (1997).
13. Shalabi, M. A., Zaidi, S. A., and Alsaleh, M. A., *Chem. Eng. Commun.* **157**, 23 (1997).
14. Kim, J. H., Suh, D. J., Park, T. J., and Kim, K. L., *Appl. Catal. A* **197**, 191 (2000).
15. Aksoylu, A. E., and. Onsan, Z. I., *Appl. Catal. A* **164**, 1 (1997).
16. Ito, M., Tagawa, T., and Goto, S., *Appl. Catal. A* **177**, 15 (1999).
17. Wang, S., and Lu, G. Q. M., *Appl. Catal. B* **16**, 269 (1998).
18. Chen, Z. X., Wu, Q. L., Li, J. L., and Zhu, Q. M., *Catal. Today* **30**, 147 (1996).
19. Wang, X., Zhao, B., Jiang, D., and Xie, Y., *Appl. Catal. A* **188**, 201 (1999).
20. Ruckenstein, E., and Hu, Y. H., *J. Catal.* **161**, 55 (1996).
21. Brunelle, J. P., *Pure Appl. Chem*. **50**, 1211 (1978).
22. Vedrine, J. C., Hollinger, G., and Minh, O. T., *J. Phys. Chem.* **82**, 1515 (1978).
23. Wu, M., and Hercules, D. M., *J. Phys. Chem.* **83**, 2003 (1979).
24. Gavalas, G. R., Phichitkul, C., and. Voecks, G. E., *J. Catal.* **88**, 54 (1984).
25. Salagre, P., Fierro, J. L. G., Medina, F., and Sueiras, J. E., *J. Mol. Catal. A* **106**, 125 (1996).
26. Zielinski, J., *J. Catal*. **76**, 157 (1982).
27. Richardson, J. T., and Crump, J. G., *J. Catal.* **57**, 417 (1979).
28. Bartholomev, C. H., and Sorensen, W. L., *J. Catal.* **81**, 131 (1983).
29. Vaarkamp, M., Miller, J. T., Modica, F. S., and Koningsberger, D. C., *J. Catal.* **163**, 294 (1996).
30. Chen, Y. G., and Ren, J., *Catal. Lett.* **29**, 39 (1994).
31. Ross, J. R. H., and Steel, M. C. F., *J. Chem. Soc., Faraday Trans*. **69**, 10 (1973).
32. Alejandre, A., Medina, F., Salagre, P., Fabregat, A., and Sueiras, J. E., *Appl. Catal. B* **18**, 307 (1998).
33. Ross, J. R. H., Steel, M. C. F., and. Isfahani, A. Z., *J. Catal*. **52**, 280 (1978).
34. Ealet, B., Gillet, E., Nehasil, V., and Moller, P. J., *Surf. Sci*. **318**, 151 (1994).
35. Shalvoy, R. B., Reucroft, P. J., and Davis, B. H., *J. Vac. Sci. Technol*. **17**, 209 (1980).
36. Solcova, O., Jiratova, K., Ueiker, D. C., and Steinike, U., *Appl. Catal.* **94**, 153 (1993).
37. Alzamora, L. E., Ross, J. R. H., Kruissink, E. C., and Van Reijen, L. L., *J. Chem. Soc., Faraday Trans.* **77**, 665 (1981).
38. Gavalas, G. R., Phichitkul, C., and Voecks, G. E., *J. Catal.* **88**, 54 (1984).
39. Stakheev, A. Yu., and Kusov, L. M., *Appl. Catal. A* **188**, 3 (1999).
40. Houalla, M., and Delmon, B., *J. Phys. Chem*. **84**, 2194 (1980).
41. Lo Jacono, M., Schiavello, M., and Cimino, A., *J. Phys. Chem.* **75**, 1044 (1971).
42. Akhmedov, V. M., Al-Khowaiter, S. H., Akhmedov, E., and Sadikhov, A., *Appl. Catal. A* **51**, 181 (1998).
43. "Merck Index," 12th ed. Merck, Rahway, NJ, 1996.
44. Ulmann, D. R., Weinberg, M. C., and Teowee, G., *J. Non-Cryst. Solids* **100**, 154 (1988)
45. Schneider, M., and Baiker, A., *Catal. Rev.—Sci. Eng.* **37**, 515 (1995).
46. Cauqui, M. A., and Rodriguez-Izquierdo, J. M., *J. Non-Cryst. Solids* **147–148**, 724 (1992).
47. Badalyan, A., Pendleton, P., and Wu, H., *Rev. Sci. Instr.* **72**, 3038 (2001).
48. Barrett, E. P., Joyner, L. G., and Halenda, P. P., *J. Am. Chem. Soc.* **73**, 373 (1951).
49. Leofarrti, G., Padovan, M., Tozzola, G., and Venturelli, B., *Catal. Today* **41**, 207 (1998).
50. Haines, P. J., "Thermal Methods of Analysis," lst ed., p. 166. Chapman & Hall, London/New York, 1995.
51. Molina, R., and Poncelet, G., *J. Catal.* **173**, 257 (1998).
52. Bogdanchikova, N. E., Fuents, S., Avalos-Borjoa, M., Farias, M. H., Boronia, A., and Dioz, G., *Appl. Catal. B* **17**, 221 (1998).
53. Ahmed, K., and Mistry, P., *Collect. Czech. Chem. Comun.* **57**, 2073 (1992).
54. Narayanan, S., and Uma, K., *J. Chem. Soc., Faraday Trans.* **81**, 273 (1985).
55. Kaliaguine, S., Adnot, A., and Lemay, G., *J. Phys. Chem*. **91**, 2886 (1987).
56. Fan, Y., Kuang, W., Zhang, W., and Chen, Y., *in* "3rd World Congress on Oxidation Catalysis" (R. K. Grasselli, S. T. Oyama, and A. M. Goffney, Eds.), Vol. 110, p. 903. Elsevier Science, Amsterdam, 1997.
57. Cho, I. H., Park, S. B., Cho, S. J., and Ryoo, R., *J. Catal.* **173**, 295 (1998).
58. Zielinski, J., *Appl. Catal.* **94**, 107 (1993).
59. Lamber, R., and Schulz-Ekloff, G., *J. Catal*. **146**, 601 (1994).